Journal of Materials Chemistry A

Valence-to-core X-ray Emission Spectroscopy of Vanadium Oxide and Lithiated Vanadyl Phosphate Materials

Journal:	*Journal of Materials Chemistry A*
Manuscript ID	TA-ART-04-2020-003620.R2
Article Type:	Paper
Date Submitted by the Author:	02-Jul-2020
Complete List of Authors:	Jahrman, Evan; National Institute of Standards and Technology, Materials Measurement Laboratory; University of Washington, Physics Holden, William; University of Washington, Physics Govind, Niranjan; Pacific Northwest National Laboratory, Environmental Molecular Sciences Laboratory Kas, Joshua; University of Washington, Physics Rana, Jatinkumar; Binghamton University, Physics, Applied Physics and Astronomy Piper, Louis; Binghamton University, State University of New York, Department of Physics, Applied Physics, and Astronomy Siu, Carrie; State University of New York at Binghamton, Whittingham, M.; Binghamton University, NECCES Fister, Tim; Argonne National Laboratory, Chemical Sciences and Engineering Seidler, Gerald ; University of Washington, Physics

Valence-to-core X-ray Emission Spectroscopy of Vanadium Oxide and Lithiated Vanadyl Phosphate Materials

Evan P. Jahrman[1](ж), William M. Holden[1], Niranjan Govind[2](†), Joshua J. Kas[1], Jatinkumar Rana[3], Louis F. J. Piper[3,4], Carrie Siu[5], M. Stanley Whittingham[5], Timothy T. Fister[6], and Gerald T. Seidler[1](‡)

[1]Physics Department, University of Washington, Seattle, WA 98195-1560, United States
[2]Environmental Molecular Sciences Laboratory, Pacific Northwest National Laboratory, Richland, WA 99354, United States
[3]Physics Department, Binghamton University, State University of New York, Binghamton, New York 13850, United States
[4]Materials Science and Engineering, Binghamton University, State University of New York, Binghamton, New York 13850, United States
[5]NorthEast Center for Chemical Energy Storage, Binghamton University, State University of New York, Binghamton, New York 13850, United States
[6]Chemical Sciences and Engineering Division, Argonne National Laboratory, Lemont, IL 60439, United States

Abstract

We report valence-to-core (VTC) X-ray emission spectroscopy (XES) measurements and theoretical calculations of the electrochemical sequence ε-$VOPO_4$, ε-$LiVOPO_4$, ε-Li_2VOPO_4 and the reference oxides V_2O_3, VO_2, and V_2O_5. In our analysis of these results, we establish a framework for interrogating chemical bonding that is generally applicable to a wide range of systems, including complex, extended inorganic compounds. While this latter regime has garnered less focused application than, e.g., metalloenzymes in many excellent catalysis studies, we show that the technique provides high utility in materials-focused energy storage research. Here, sensitivities to the local atomic structure and hybridization schemes are discussed in detail. Similarly, the effect of lithiation on oxidation, delocalization, and shifts in ligand valence energy levels are all readily apparent in the analyzed results. Finally, the TDDFT projections clearly reveal the directional dependencies of the valence band at each of the vanadium sites.

Our results demonstrate laboratory-based X-ray spectroscopy instrumentation is a viable route for attaining well-resolved VTC-XES features for inorganic compounds of 3d transition metals, even for samples of limited quantity or suffering from sensitivity to the atmosphere. The experimental results are in good agreement with results produced by real-space Green's function and time-dependent density functional theory (TDDFT) methods, respectively. Hence, we propose that VTC-XES, when equipped with appropriate theoretical support, can be a valuable complement to X-ray absorption pre-edge features for more detailed characterization of a compound's electronic structure. We expect similar analyses will find application in a broad range of materials chemistry research and provide both fundamental and applied insights.

(ж) evan.jahrman@nist.gov - author is currently at the National Institute of Standards and Technology in Gaithersburg, MD ; (†) niri.govind@pnnl.gov ; (‡) seidler@uw.edu

1. Introduction

This article presents a combined experimental and theoretical study of valence-to-core (VTC) X-ray emission spectroscopy (XES) measurements of a suite of lithiated ε-phase vanadyl phosphate compounds and a suite of reference vanadium oxides. This is motivated by the overlapping considerations of four main topics spanning: materials interest; energy storage science; instrument development; and the need to test and validate the predictions of electronic structure theory.

First, from a materials perspective, lithiation of vanadyl phosphates is an area of ongoing research due to its promise as a next-generation cathode material in lithium ion batteries (LIBs).[1-3] Likewise, vanadium oxides are frequently recommended for societally-critical applications including data and energy storage devices.[4-10] The materials studied here span all accessible oxidation states of vanadium oxides and vanadyl phosphates. In order, V_2O_3 has been proposed as a candidate material for energy storage applications.[7] VO_2 has been extensively studied in both pristine and doped conditions.[11-13] This material undergoes a metal-to-insulator phase transition at 341 K, not far above room temperature,[14, 15] and as a result it is has been investigated as a candidate switching material for data storage devices.[6, 8, 9] V_2O_5 is frequently used in energy applications spanning a range of power and energy densities. On one end of this range of applications, V_2O_5 is an inexpensive and effective electrode material in supercapacitors,[5, 16-18] while on the other end, V_2O_5 and its derivatives are candidate cathode materials both for lithium intercalation[19-22] and for magnesium ion batteries.[4, 23, 24] For the other class of materials, vanadyl phosphates have been proposed as a candidate cathode material for lithium ion batteries, as noted above.[2, 3] The attractive feature of vanadyl phosphates is their

ability to accommodate multiple lithium ions for each vanadium host. Moreover, it is one of the few materials that can do this via an intercalation rather than a conversion process with redox potentials for both electrochemical conversions at relatively high potentials. As a result, its theoretical capacity is 305 mAh g^{-1} and exceeds that of conventional layered oxide cathodes derived from $LiCoO_2$.[1, 25] Moreover, recent progress has been made in synthesizing vanadyl phosphate cathode materials as well as achieving reversible cycling and improved capacities.[1, 26, 27] Indeed, the accurate oxidation state analysis was critical in determining how ball-milling induced disorder was exacerbating poor kinetics in the high-voltage regime of Li_xVOPO_4,[28] which was later circumvented by synthesizing nanoparticles of $VOPO_4$ within a graphene matrix.[1] Accordingly, synthesized vanadyl phosphates cathodes can reasonably achieve practical capacities around the theoretical value. This contrasts with $LiCoO_2$ cathode derivatives which require incomplete insertion and extraction of lithium to maintain reversible cycling. Hence, the lithiated vanadyl phosphates are promising materials with electronic structures of great interest, albeit with nontrivial atomic structures. Thus, on the basis of their technological motivation and also the relatively high complexity of the coordination of the metal ion, the compounds studied here represent excellent candidates for VTC-XES analysis and exploration of theoretical methods.

Second, from a spectroscopy-oriented perspective, VTC-XES is a powerful technique that has garnered substantial interest, especially for 3d transition metals.[29-31] In particular, the Kβ'' for 3d transition metals is frequently analyzed due to its sensitivity to the identity of neighboring atoms.[30] However, VTC-XES also permits the element-specific investigation of valence electronic structure. Therefore, it is desirable to further establish this technique as a general tool for studying molecular bonding in a wide range of materials. However, with a few

notable exceptions,[32-34] VTC-XES has primarily been applied to the study of metallo-organic complexes and catalysts.[35-37] For example, many researchers attempted to elucidate the atomic identity of a light central atom in FeMoCo, the active site for binding and reduction in nitrogenase, reported by Einsle *et al.*,[38] but it was not until Lancaster *et al.* used Fe VTC-XES that the atom was experimentally established to be carbon.[39] Similarly, Fe VTC-XES has also been applied to a number of doubly nitrogenous Fe compounds which spanned a range of N-N bond distances.[40] Pollock *et al.* found that the position of a feature corresponding to the σ_{2s2s}* $\rightarrow$ Fe_{1s} transition could be used to track the N-N bond distance and thus the degree of activation in Fe-based catalysts used for nitrogen reduction. Other notable examples in VTC-XES include the work of Pushkar *et al.* who utilized Mn VTC-XES to interrogate the electronic structure of the Mn_4Ca cluster in the oxygen evolving complex of photosystem II.[41] With VTC-XES, these researchers were able to detect oxygen ligation to the Mn_4Ca cluster. Elsewhere, the sensitivities of the Kβ'' peak have been well documented by a study spanning a collection of manganese oxides.[42] Recently, Cutsail *et al.* furthered the investigation of O-O activation by using VTC-XES to study Cu_2O_2-based catalysts.[43] Beyond catalysis research, the VTC-XES of numerous Cr compounds were analyzed by experimental and theoretical means and were found to exhibit considerable sensitivity to the particular coordination of the Cr atoms in the system, albeit with limited utility in speciation determination.[44] Finally, VTC-XES has been used to discriminate amongst members of a set of Mn^{IV} dimers with varying protonation states on bridging oxygen atoms.[45] Nevertheless, much work remains to be done in measuring, cataloguing, and calculating the VTC-XES spectra of chemical species. For this application, modern laboratory-based X-ray spectrometers are particularly well-suited, as is demonstrated in prior work by some of the present authors[46, 47] and others.[48]

Third, there has been ample recent growth in the capabilities, diversities of design, and operational energy ranges of laboratory-based instruments for nonresonant XES and related spectroscopies.[46, 49-54] Laboratory-based spectrometers can measure tender X-ray energies (such as S and P K emission lines at ~ 2-2.5 keV) using double crystal monochromators,[55-57] dispersive Rowland circle geometries,[58-61] or the von Hamos geometry.[62] In contrast, Laue-type spectrometers can access higher energies, including Au Kβ lines (78 keV).[63] In the ~3-12 keV range, many existing von Hamos instruments have been used for studies of first row transition metals and lanthanides.[49, 64-66] For similar energies, Rowland circle-based configurations using spherically bent crystal analyzers (SBCAs) have been extensively developed by some of the present authors.[47, 54, 67-71] Most of these spectrometers use conventional fixed anode X-ray tube sources which emit broadband radiation. For XES measurements in particular, this broadband flux can be especially efficiently utilized, particularly when so-called 'X-ray fluorescence' (XRF) style tubes are used.[54] Consequently, these spectrometers yield core-hole creation rates that are a significant fraction of those for a monochromatized insertion device at a 3rd generation synchrotron light source. Moreover, the instruments employ SBCAs that yield excellent energy resolution, unsurprisingly, as this is also the most common optic used for high-resolution hard X-ray spectroscopy at synchrotron X-ray sources. Thus, spectra are achieved in the laboratory without loss in instrumental resolution compared to synchrotron implementations, but with the limitation that the XES spectrum of a material must be measured nonresonantly. Indeed, such instrumentation is rapidly developing and is beginning to aid in studies of energy-related and catalyst materials.[5, 72-74]

Fourth, setting the stage for testing of theoretical tools, we show below that many of the vanadyl phosphates possess complex VTC-XES spectral features. This is analogous to the VTC-

XES of several molecular systems which, because of their relatively complex structure, possess notably complex VTC-XES signatures.[75-77] In contrast, many inorganic 3d transition metal compounds exhibit a relatively structureless VTC-XES feature next to a single Kβ'' feature.[35, 39, 42, 43, 47] Accordingly, the measurements reported here are excellent test cases to verify theoretical models which simulate the XES process in extended inorganic systems. In particular, TDDFT has emerged as a favorable alternative to a simple, single-electron DFT framework, where initial core hole and final valence ionized states are both represented by single Slater determinants constructed with Kohn-Sham (KS) orbitals.[47, 78-81] In contrast, TDDFT permits the calculation of properties in the presence of external potentials, including those by time-varying electric fields. Indeed, electronic transitions arise naturally in this formalism as the roots of the Kohn-Sham response function. Moreover, these excited states are, in general, composed of contributions from many determinants. This is a definite advantage over conventional DFT approaches, particularly for transition metals, which are notorious for possessing many states closely spaced in energy such that the promotion and pairing energy of valence electrons become of comparable size. Furthermore, in the `NWChem` implementation[81, 82] the calculated roots span electric dipole, electric quadrupole, and magnetic dipole contributions to the oscillator strength corresponding to the transition. These merits resulted in excellent spectral agreement between Zn VTC-XES calculations and experimental results for a variety of chemistries for inorganic compounds[47] and has recently shown similarly high quality agreement with the VTC-XES for a broad range of sulfur containing compounds.[83] Furthermore, TDDFT has been used to accurately model the X-ray absorption near edge structure (XANES) and VTC-XES of many materials, including transition metal compounds.[80, 81, 84-88] Here, we find excellent agreement between theory and experiment, but require considerable care in, e.g., the construction of the crystalline cluster

models. The TDDFT results are compared to real-space Green's function calculation via `FEFF9` and the accuracy of each is evaluated. Finally, our TDDFT results are further analyzed by identifying the atomic contributions to each spectral range and the projection of the dipole operator's matrix elements along several chemical bonds. These approaches possess several advantages for solid state systems, as will be discussed in the context of the extended inorganic compounds studied here.

2. Methodology

Compounds

All vanadium oxides were purchased from commercial vendors. Specifically, V_2O_3 and VO_2 were acquired from Alfa Aesar while V_2O_5 was acquired from Sigma-Aldrich. The purity of each compound was at least 95 percent. Moreover, the phase and speciation of each was confirmed by X-ray diffraction (XRD) and XANES, respectively. XRD permitted the phases of each oxide to be confirmed by matching the measurements to experimental spectra from a commercially available database of the International Center for Diffraction Data (ICDD). XANES confirmation was done by comparison to literature spectra.[89-91] The ε-$VOPO_4$ and its lithiated phases were prepared at Binghamton University by methods reported elsewhere.[1] The phases of ε-$VOPO_4$ and ε-$LiVOPO_4$ were again confirmed by matching the measurements to experimental XRD spectra from the ICDD database. A Li_2VOPO_4 entry could not be located in this same database. Rather, the structure reported by Bianchini *et al.*[92] was used to simulate an XRD spectrum using the `xrayutilies`[93] package for Python and confirmed to match the spectrum measured for the ε-Li_2VOPO_4 measured here.

The following steps were taken to prepare samples for X-ray analysis. The lithiated vanadyl phosphates, which are known to be air sensitive, were placed in vials and shipped in

sealed aluminum mylar bags flushed with inert gas. The vials were eventually opened in an argon glovebox at the University of Washington. The material was spread into a thin layer and sealed between three layers of polyimide tape with a silicon-based adhesive. These materials were then placed into a vial and sealed with parafilm prior to removal from the glovebox. These vials were opened immediately prior to measurement. The VTC-XES results, coupled with a V $K\beta_{1,3}$ spectrum measured at the start of each VTC-XES scan, were monitored over numerous scans to confirm that no degradation occurred. The material was measured by XRD after XES acquisition had completed to confirm each phase remained intact. The pristine ε-$VOPO_4$ was dried in a vacuum oven overnight to remove any hydrated or hydroxide components from the material. This was confirmed by XRD and the ε-$VOPO_4$ was also sealed by polyimide tape prior to measurement.

XES Experiment

A laboratory-based spectrometer at the University of Washington was used for these experiments. The basic design of the instrument is described in Seidler *et al.*[54] and the advances of Jahrman *et al.*[46] were utilized. We used a Ge(422) spherically bent crystal analyzer (SBCA) which was aligned according to the method of Mortensen *et al.*[70] The energy resolution and scale was maintained by a slit on the sample side[47, 69] which each sample was aligned behind. In addition to these details, the instrument configuration included a Varex VF80 X-ray tube source which was operated at a total tube power of 100 W and with a tungsten anode. A commercial SDD (Amptek X-123SDD) served as the final detector and provided sufficient energy resolution to exclude much of the background fluorescence and other stray scatter.

For the data collection and analysis, VTC-XES spectra were averaged over several scans spanning an energy range from 5390 to 5500 eV to capture both the V Kβ mainlines and V VTC-

XES. The total integration time for each scan was approximately 7 minutes, while the total measurement time for a sample was typically around 4 hours so as to obtain data with extremely high signal-to-noise, i.e., so that Poisson noise was fairly negligible in the final spectra. All spectra were deadtime corrected, background subtracted and integral normalized over the full range of the spectrum. To aid comparison to theory, the high energy tail from the V $K\beta_{1,3}$ of each sample was subtracted from its VTC-XES spectrum. In principle, this can be done by conventional peak-fitting methods. However, for XES features, this would require robust predictions of the presence and shape of radiative Auger emission features[94] and multielectron excitation satellites.[67] Furthermore, it can be difficult to meaningfully constrain the physical parameters contributing to the shape of each feature, and with many free parameters, it is difficult to obtain a unique fit to the experimental data. Alternatively, approximate parameters can be used to fit a set of Lorentzians to the slope on the low-energy side of the VTC-XES spectrum from the V $K\beta_{1,3}$ and another set fit to the tail on the high-energy side. This shape may be subtracted from the experimental spectrum to produce a flat-baseline spectrum that, while it may possess small inaccuracies in the relative intensity of features, is devoid of distortions that might appear as false additional VTC-XES features.

XES Theory

VTC-XES results were modeled using `NWChem`.[82] The input cluster models were constructed from experimental configurations which were accompanied by XRD spectra in agreement with those measured here. These clusters were truncated to a convenient size and the surface of the resulting cluster was terminated by pseudohydrogen or fractionally charged hydrogen atoms.[47, 87, 95-97], resulting in capped clusters of approximately 100-150 atoms. With an appropriate atomic input constructed, XES calculations were carried out by the following

established method.[81, 98] First a DFT calculation was performed on the ground state system with the PBE0[99] exchange correlation functional. The following basis sets were used for each element: H used LANL2DZ,[100] Li used 6-31G*,[101, 102] P and O used the effective core potential basis Stuttgart RLC ECP,[103] and V used the effective core potential basis LANL2DZ ECP[104] except on the photoexcited atom which used Sapporo TZP 2012.[105] The pentavalent vanadium complexes were treated as diamagnetic compounds while all others were modeled as high spin paramagnets.[106-109] Second, the converged molecular orbital vectors were used as input for a full core hole calculation[110-112] to optimize the electronic structure in the presence of the core hole subject to a maximum overlap condition as implemented in NWChem.[113, 114] Third, this solution was then used as the input to the TDDFT calculation, which was performed in the Tamm-Dancoff approximation.[115]

The above calculations provided energies and oscillator strengths for a number of electronic transitions. Processing these into a meaningful spectrum required the following steps. The oscillator strengths in the channels corresponding to excitation of a spin-up or spin-down electron in the V_{1s} orbital were normalized to give equal weight to both channels subject to the assumption that ejection of either electron was equally probable, and that excitation was the rate-limiting step in the photoexcitation process. Oscillator strengths were rescaled to probabilities according to the formulae given by Mukoyama.[116] Each transition line was convolved with a 0.99 eV full-width half-maximum (FWHM) Lorentzian and the sum of all Lorentzians was taken as the final spectrum. In order to characterize the contribution of a given atomic orbital-type to a transition, the corresponding oscillator strengths were scaled by the contributions of molecular orbital pairs involved in the corresponding root found by TDDFT. These molecular orbital

contributions were then scaled according to the contributions of the individual atomic orbitals, and the results were binned by atomic orbital-type.

For comparison, the FEFF9[117-119] real-space multiple-scattering code was also used to calculate the vanadium Kβ emission as well as the angular momentum projected densities of states (LDOS) of each compound. The code treats XES in terms of matrix elements between the core-level and the Green's function, i.e.,

$$\sigma_{XES}(\omega) \propto \langle c|d^{*}\,G(\omega + E_c)d|c\rangle\theta(\mu - \omega - E_c), \quad (1)$$

where $|c\rangle$ denotes the single particle core-state, d is the transition operator (usually dominated by dipole transitions), E_c is the core-level energy, and G is the one electron Green's function. The unit step function $\theta(\mu - \omega - E_c)$ selects occupied levels below the chemical potential μ.

For these calculations, potentials and densities were calculated with the self-consistent field (SCF) approach with a SCF radius of 5.0 Å, leading to a cluster ranging from 40 to 60 atoms. A full multiple scattering radius of approximately 8.5 Å (a cluster of 200-300 atoms) was used in the calculation of the LDOS and the XES and was sufficiently large to produce a converged spectrum. Core-hole effects were neglected, other than the core-hole lifetime broadening, which was introduced as a shift into the complex plane of the energy at which the Green's function is evaluated and is equivalent to a Lorentzian broadening of 0.99 eV FWHM.

3. Results and Discussion

The VTC-XES measurements reported in Fig. 1 exhibit multiple trends which are well-known[42] and have been verified for several classes of vanadium compounds.[120] First, a Kβ'' feature corresponding to the "cross-over" transition from a molecular orbital of predominantly ligand character is clearly visible in most spectra. The Kβ'' is of variable intensity and decreases in intensity as expected from the known changes in V-O bond distances.[121-123] This is apparent

for both the oxides and phosphate-based compounds. Second, the $K\beta_{2,5}$ position is also observed to be highly sensitively to oxidation state, with the more oxidized found at higher emission energies. Third, a slight curvature is present on the high energy side of the spectra in Fig. 1 and is a result of the spectra being truncated along a multi-electron excitation feature which is outside the scope of this study. Finally, an interesting triple-peak structure is observed in the main bonding-derived VTC feature of all the vanadyl phosphates.

In Fig. 2, a background and residual are shown for the fit of a representative VTC-XES spectrum. The fit is observed to agree well with the high-energy tail from the $K\beta_{1,3}$. The background stays below the VTC-XES features, and, likewise, does not exceed the majority of the multi-electron excitation feature around 5480 eV. Toward the highest energies, the fitted background is converging to the measured VTC-XES spectrum, as expected. Similar fits were performed for all compounds and the resulting background-subtracted spectra are used in all other figures.

In Fig. 3 and Fig. 4, theoretical Green's function and TDDFT calculations are shown relative to the measured experimental spectra. In all cases, the TDDFT calculations required a constant energy shift of -29 eV to align with the experimental spectra. For the calculations performed in `FEFF9`, all the oxides required a uniform energy shift to align to experiment, while each of the vanadyl phosphates required individual energy shifts to achieve satisfactory alignment. Both theories qualitatively capture the spectral features in the VTC-XES, including the triple-peak structure of the $K\beta_{2,5}$ feature for the vanadyl phosphates. For several compounds, including VO_2 and V_2O_3, TDDFT provides better predictions for the energy spacing of the Kβ'' and $K\beta_{2,5}$ features, and also a more accurate prediction of the high-energy behavior of the $K\beta_{2,5}$ features around 5463 eV in the oxides.

Both NWChem and FEFF9 offer methods for assessing the underlying character of the observed spectral features. In FEFF9, this can be accomplished by investigating various contributions to the system's density of states. In NWChem, the character of each feature can be assessed by investigating the contribution of each type of atomic orbital to the transitions forming that feature. Indeed, this process has proven to be a valuable tool for interpretation in prior work.[124, 125] Here, as many transitions were predicted by TDDFT, it is useful to sort them into several energy bins. In order to limit assumptions about the characteristics of the observed features, these bins were chosen to approximately encompass each of the major predicted features. Starting with Fig. 5, it is apparent that the largest contribution to the intensity of the Kβ'' comes from orbitals of O(s) (O(s) = oxygen *s*-type angular momentum basis orbitals) character. While this agrees with conventional analyses that attribute this feature to "cross-over" transitions from valence s-type ligand orbitals,[31, 35, 126, 127] the results exhibit many trends that reveal more complexity than this simple picture. For example, O(s) character is observed in all regions. Towards higher energies, the O(p) contributions increase, again as expected.[40] However, notable V contributions are present, many of which are likely hybridized orbitals with traditionally dipole-allowed orbitals. This is in agreement with predictions of extensive hybridization in transition metal oxide systems,[128-130] especially between V 3d and O 2p orbitals.[131] Indeed, classic crystal field texts have shown the relative complexity and hybridization of even isolated clusters of the V_2O_5 complex.[132] Many of these same trends are observed in the vanadyl phosphates shown in Fig. 6. Again, strong O(p) contributions are observed throughout each spectrum, while the O(s) contributions peak in the Kβ'' feature. Likewise, various V orbitals maintain some involvement throughout each of the spectra. Unlike the pure oxides, a substantial degree of P(s), P(p), Li(s) and Li(p) are observed in different

regions of the main VTC-XES feature. As VTC-XES is a local probe, it reflects the components of orbitals in the immediate vicinity of the metal center. In this way, diffuse or delocalized orbitals are still able to contribute some strength to the observed transitions. Consequently, VTC-XES retains some sensitivity to changes in functional groups and delocalized orbitals. Here, none of the P or Li atoms are directly associated with the absorbing V atom. Therefore, the observed transitions indicate some delocalization of the molecular orbitals in the valence band. Specifically, the growing Li(s) and Li(p) contributions upon lithiation, along with the fact that Li(p) contributions would not be possible in the electronic configuration of atomic Li, reveals a growing hybridization between the valence band of the vanadyl phosphate and the intercalated Li atoms. While the present analysis is particular to the results obtained for lithiated vanadyl phosphates, the methodology is not. Rather, this framework is amenable to other energy storage materials and the discussed sensitivities can be applied to understanding their relevant performance metrics. Indeed, strictly considering Li-ion cathodes: orbital hybridization plays a key role in achieving high capacities without compromising stable redox cycling,[133] localization is known to substantially impact delithiation voltages,[134] and tracking ligand valence electrons is often critical to the elucidation of complex charge compensation mechanisms.[135]

At this point, further insights regarding the origin of the VTC-XES can be attained by carefully considering the directional dependence of the transition dipole operator. Note that for molecular systems, this is generally done by selecting the most prominent molecular orbitals as identified by calculations in a single-particle theoretical framework. However, simulating a solid state system's VTC-XES features with TDDFT often returns a large number of transitions, as can be seen in Figures 5 and 6, and these transitions may well involve significant contributions from many molecular orbitals. This makes a systematic identification of the prominent

molecular orbitals by parsing the predicted roots inadvisable. Rather, we explore an alternative method motivated by a few innovative studies on single crystal systems which used core-to-core XES spectra acquired at multiple angles to assess crystal field shifts and linear dichroism in the systems of interest.[136, 137] Fundamentally, this behavior is due to the interaction between the cartesian components of the dipole operator and the symmetry or polarization of the system. As such, some VTC-XES features of highly symmetric molecules have been successfully analyzed by invoking group theoretical arguments to predict the angular dependent suppression of molecular orbital contributions according to the underlying irreducible representations.[136, 138] Here, we extend the directional arguments of Pollock *et al.*[139] to show that these projections can be made quite generally to selectively explore the nature of bonds in solid state systems of lower symmetry. Specifically, the VTC-XES features in this work are further analyzed by projecting the transition dipole moment along the direction of three unique bonds in each compound.

Applying the above approach to the pure oxides yields the results shown in Fig. 7. The projections were done using directional cosines between the transition dipole moment direction and the projection directions. Note that these axes are non-orthogonal and the resulting decomposition is not expected to sum to the calculated VTC-XES spectrum. In the case of VO_2 and V_2O_3, each V-O bond is roughly equivalent and the resulting projections demonstrate moderate differences which may be attributed to the imperfect symmetry of the truncated cluster used in the calculation. For V_2O_5, it can be seen that the Kβ'' is dominated by the transitions with dipole moments along the direction of the vanadyl oxygen. This is reasonable as the vanadyl oxygen is closest to the V center and the intensity of the Kβ'' feature is known to depend exponentially on the distance to the neighboring atoms.[42] Interestingly, this projection does not dominate the main VTC-XES feature. In Fig. 8, similar projections are shown for the

vanadyl phosphates. A few trends merit mention. First, the Kβ'' feature is again dominated by the vanadyl oxygen; however, contributions can be seen along other directions. Moreover, there is a monotonically growing energy separation between the projections in the vanadyl and non-vanadyl oxygen directions in this region. While it should be noted that orthogonality of the projection directions is not enforced, this trend suggests that the gap between the energy of the associated ligand valence electrons is likewise broadened upon lithiation. In the main VTC feature, the lowest energy peak in the observed triplet feature is captured by projection in the direction of the oxygens belonging to the phosphide groups. The next highest energy peak in the triplet is primarily composed of these same projections, but often with some component from the vanadyl oxygen, especially in the case of the $LiVOPO_4$ simulations. Finally, the highest energy peak in the triplet feature of the vanadyl phosphates can be seen to be primarily due to the projection of the dipole along the direction of the vanadyl oxygen. While these projections only probe those states which are able to participate in dipole transitions to the 1s core hole on the central V atom, it is still suggestive of the relative energies of molecular orbitals composing the valence band. Again, while the above discussion was particular to the results obtained for the suite of vanadium-based compounds considered here, the methodology is flexible. Indeed, the present directional analysis is relevant to broader classes of energy storage materials where it is generally recognized that diverse bonding schemes strongly influence the redox processes. As an example, multiple local oxygen environments are found in Li-excess materials and the density of states around each of these states is closely related to the oxygen redox activities providing improved cathode capacities.[140]

A final note should be made in discussing the present results. Namely, that there is an impressive body of prior work on vanadium oxide materials in the soft X-ray regime.[141-143]

There, one advantage is access to both the V L-edges and the O K-edge which aids in selectively interrogating the system. In contrast, the present study uses instrumentation optimized for the hard X-ray regime to probe VTC-XES features near the V K-edge. Due to selection rules, it can then be deduced that our approach provides access to a different projection of the density of states than is usually interrogated in the soft X-ray regime. Furthermore, there are several practical advantages in using higher energy photons. Specifically, this approach naturally leads to increased bulk sensitivity and can therefore serve as a useful complement to surface sensitive spectroscopies. Indeed, this property has proven particularly valuable in studies using the same instrumentation to analyze nanoscale energy storage materials as it helps provide a better understanding of the spatial dependence of speciation in the system.[5, 16, 17, 144, 145] Moreover, the present energy regime provides greater flexibility in experimental design. For example, not only can these measurements be done under ambient pressures, but the present methodology can be extended to future VTC-XES studies on energy materials under *in situ* conditions. Indeed, parallel work has already been performed using laboratory-based instrumentation to perform rapid XANES measurements around several transition metal K-edges to analyze a working pouch cell battery under industrially relevant charging rates.[146]

4. Conclusion

The VTC-XES of several compounds of societal and scientific relevance have been measured and presented. The complex structure of the VTC-XES of the vanadyl phosphates suggests that the relative lack of distinct features that has previously been reported in many VTC-XES for inorganic crystalline states is due to the high symmetry and overall simplicity of their bonding, rather than due to a lack of sensitivity from VTC-XES. Furthermore, the high quality of reported spectra clearly supports the utility of laboratory-based X-ray spectroscopy instrumentation for

the measurement of VTC-XES of 3d transition metal compounds. Likewise, modern computational procedures reproduced the experimental spectra with good agreement, further establishing these techniques for the modeling and interpretation of VTC-XES results. This manuscript serves as a framework for future studies investigating the electronic structure of low-coordination-symmetry inorganic materials by VTC-XES with laboratory-based X-ray spectroscopy instrumentation.

5. Conflicts of Interest

There are no conflicts of interest to declare.

6. Acknowledgements

EPJ and TTF were supported in part by the Joint Center for Energy Storage Research (JCESR), an Energy Innovation Hub funded by the U.S. Department of Energy, Office of Science, and Basic Energy Sciences. EPJ was also supported by a subcontract from the National Institute of Standards and Technology. Opinions, recommendations, findings, and conclusions presented in this manuscript and associated materials does not necessarily reflect the views or policies of NIST or the United States Government. Part of this work was conducted at the Molecular Analysis Facility, a National Nanotechnology Coordinated Infrastructure site at the University of Washington which is supported in part by the National Science Foundation (grant NNCI- 1542101), the University of Washington, the Molecular Engineering & Sciences Institute, and the Clean Energy Institute. This material is based in part upon work supported by the State of Washington through the University of Washington Clean Energy Institute. The work of J. Rana, L. F. J. Piper, C. Siu, and M. S. Whittingham was supported as part of the NorthEast Center for Chemical Energy Storage (NECCES), an Energy Frontier Research Center funded by the U.S. Department of Energy, Office of Science, Basic Energy Sciences under Award No. DE-SC0012583. NG acknowledges support from the U.S. Department of Energy, Office of Science,

Office of Basic Energy Sciences through Award No. KC030105172685. This research benefited from computational resources provided by the Environmental Molecular Sciences Laboratory (EMSL), a DOE Office of Science User Facility sponsored by the Office of Biological and Environmental Research and located at PNNL. PNNL is operated by Battelle Memorial Institute for the United States Department of Energy under DOE Contract No. DE-AC05- 76RL1830.

7. References

1. C. Siu, I. D. Seymour, S. Britto, H. Zhang, J. Rana, J. Feng, F. O. Omenya, H. Zhou, N. A. Chernova, G. Zhou, C. P. Grey, L. F. J. Piper and M. S. Whittingham, Chemical Communications **54** (56), 7802-7805 (2018).
2. M. S. Whittingham, Chemical Reviews **104** (10), 4271-4302 (2004).
3. M. S. Whittingham, Chemical Reviews **114** (23), 11414-11443 (2014).
4. J. L. Andrews, A. Mukherjee, H. D. Yoo, A. Parija, P. M. Marley, S. Fakra, D. Prendergast, J. Cabana, R. F. Klie and S. Banerjee, Chem **4** (3), 564-585 (2018).
5. W. Bi, E. Jahrman, G. Seidler, J. Wang, G. Gao, G. Wu, M. Atif, M. AlSalhi and G. Cao, ACS Applied Materials & Interfaces **11** (18), 16647-16655 (2019).
6. M. D. Goldflam, T. Driscoll, B. Chapler, O. Khatib, N. Marie Jokerst, S. Palit, D. R. Smith, B.-J. Kim, G. Seo, H.-T. Kim, M. D. Ventra and D. N. Basov, Applied Physics Letters **99** (4), 044103 (2011).
7. N. Hassan, J. Riaz, M. T. Qureshi, A. Razaq, M. Rahim, A. M. Toufiq and A. Shakoor, Journal of Materials Science: Materials in Electronics **29** (18), 16021-16026 (2018).
8. M. Son, J. Lee, J. Park, J. Shin, G. Choi, S. Jung, W. Lee, S. Kim, S. Park and H. Hwang, IEEE Electron Device Letters **32** (11), 1579-1581 (2011).
9. R. Xie, C. T. Bui, B. Varghese, Q. Zhang, C. H. Sow, B. Li and J. T. L. Thong, Advanced Functional Materials **21** (9), 1602-1607 (2011).
10. J. del Valle, P. Salev, F. Tesler, N. M. Vargas, Y. Kalcheim, P. Wang, J. Trastoy, M.-H. Lee, G. Kassabian, J. G. Ramírez, M. J. Rozenberg and I. K. Schuller, Nature **569** (7756), 388-392 (2019).
11. A. Krammer, O. Bouvard and A. Schüler, Energy Procedia **122**, 745-750 (2017).
12. N. Wang, M. Duchamp, R. E. Dunin-Borkowski, S. Liu, X. Zeng, X. Cao and Y. Long, Langmuir **32** (3), 759-764 (2016).
13. L. Zhao, L. Miao, C. Liu, C. Li, T. Asaka, Y. Kang, Y. Iwamoto, S. Tanemura, H. Gu and H. Su, Scientific reports **4**, 7000 (2014).
14. J. Stajic, Science **362** (6418), 1014 (2018).
15. J. H. Park, J. M. Coy, T. S. Kasirga, C. Huang, Z. Fei, S. Hunter and D. H. Cobden, Nature **500**, 431 (2013).
16. W. Bi, J. Huang, M. Wang, E. P. Jahrman, G. T. Seidler, J. Wang, Y. Wu, G. Gao, G. Wu and G. Cao, Journal of Materials Chemistry A **7** (30), 17966-17973 (2019).
17. W. Bi, J. Wang, E. P. Jahrman, G. T. Seidler, G. Gao, G. Wu and G. Cao, Small **15** (31), 1901747 (2019).
18. W. Bi, Y. Wu, C. Liu, J. Wang, Y. Du, G. Gao, G. Wu and G. Cao, ACS Applied Energy Materials **2** (1), 668-677 (2019).
19. J. S. Braithwaite, C. R. A. Catlow, J. D. Gale and J. H. Harding, Chem Mater **11** (8), 1990-1998 (1999).

20. R. Jourdani, L. Jadoual, M. Ait El Fqih, A. El Boujlaidi, H. Aouchiche and A. Kaddouri, Surf Interface Anal **50** (1), 52-58 (2018).
21. S. Nordlinder, L. Nyholm, T. Gustafsson and K. Edström, Chem Mater **18** (2), 495-503 (2006).
22. L. R. De Jesus, G. A. Horrocks, Y. Liang, A. Parija, C. Jaye, L. Wangoh, J. Wang, D. A. Fischer, L. F. J. Piper, D. Prendergast and S. Banerjee, Nature Communications **7** (1), 12022 (2016).
23. S.-C. Lim, J. Lee, H. H. Kwak, J. W. Heo, M. S. Chae, D. Ahn, Y. H. Jang, H. Lee and S.-T. Hong, Inorg Chem **56** (14), 7668-7678 (2017).
24. G. Sai Gautam, P. Canepa, A. Abdellahi, A. Urban, R. Malik and G. Ceder, Chem Mater **27** (10), 3733-3742 (2015).
25. J.-W. Lee, S.-M. Park and H.-J. Kim, Journal of Power Sources **188** (2), 583-587 (2009).
26. Z. Chen, Q. Chen, L. Chen, R. Zhang, H. Zhou, N. A. Chernova and M. S. Whittingham, Journal of The Electrochemical Society **160** (10), A1777-A1780 (2013).
27. Y. Song, P. Y. Zavalij and M. S. Whittingham, Journal of The Electrochemical Society **152** (4), A721-A728 (2005).
28. J. Rana, Y. Shi, M. J. Zuba, K. M. Wiaderek, J. Feng, H. Zhou, J. Ding, T. Wu, G. Cibin, M. Balasubramanian, F. Omenya, N. A. Chernova, K. W. Chapman, M. S. Whittingham and L. F. J. Piper, Journal of Materials Chemistry A **6** (42), 20669-20677 (2018).
29. U. Bergmann and P. Glatzel, Photosynth Res **102** (2), 255 (2009).
30. E. Gallo and P. Glatzel, Advanced Materials **26** (46), 7730-7746 (2014).
31. P. Glatzel and U. Bergmann, Coordination Chemistry Reviews **249** (1-2), 65-95 (2005).
32. S. G. Eeckhout, O. V. Safonova, G. Smolentsev, M. Biasioli, V. A. Safonov, L. N. Vykhodtseva, M. Sikora and P. Glatzel, Journal of Analytical Atomic Spectrometry **24** (2), 215-223 (2009).
33. C. Weis, G. Spiekermann, C. Sternemann, M. Harder, G. Vankó, V. Cerantola, C. J. Sahle, Y. Forov, R. Sakrowski, I. Kupenko, S. Petitgirard, H. Yavaş, C. Bressler, W. Gawelda, M. Tolan and M. Wilke, Journal of Analytical Atomic Spectrometry **34** (2), 384-393 (2019).
34. L. Hanna, P. Kucheryavy, N. Lahanas and J. V. Lockard, The Journal of Chemical Physics **150** (17), 174707 (2019).
35. E. Gallo, C. Lamberti and P. Glatzel, Physical Chemistry Chemical Physics **13** (43), 19409-19419 (2011).
36. N. Lee, T. Petrenko, U. Bergmann, F. Neese and S. DeBeer, J Am Chem Soc **132** (28), 9715-9727 (2010).
37. J. C. Swarbrick, Y. Kvashnin, K. Schulte, K. Seenivasan, C. Lamberti and P. Glatzel, Inorg Chem **49** (18), 8323-8332 (2010).
38. O. Einsle, F. A. Tezcan, S. L. A. Andrade, B. Schmid, M. Yoshida, J. B. Howard and D. C. Rees, Science **297** (5587), 1696 (2002).
39. K. M. Lancaster, M. Roemelt, P. Ettenhuber, Y. Hu, M. W. Ribbe, F. Neese, U. Bergmann and S. DeBeer, Science **334** (6058), 974 (2011).
40. C. J. Pollock, K. Grubel, P. L. Holland and S. DeBeer, J Am Chem Soc **135** (32), 11803-11808 (2013).
41. Y. Pushkar, X. Long, P. Glatzel, G. W. Brudvig, G. C. Dismukes, T. J. Collins, V. K. Yachandra, J. Yano and U. Bergmann, Angewandte Chemie International Edition **49** (4), 800-803 (2010).
42. U. Bergmann, C. R. Horne, T. J. Collins, J. M. Workman and S. P. Cramer, Chem Phys Lett **302** (1), 119-124 (1999).
43. G. E. Cutsail III, N. L. Gagnon, A. D. Spaeth, W. B. Tolman and S. DeBeer, Angewandte Chemie International Edition **58** (27), 9114-9119 (2019).
44. S. N. MacMillan, R. C. Walroth, D. M. Perry, T. J. Morsing and K. M. Lancaster, Inorg Chem **54** (1), 205-214 (2015).

45. B. Lassalle-Kaiser, T. T. Boron, 3rd, V. Krewald, J. Kern, M. A. Beckwith, M. U. Delgado-Jaime, H. Schroeder, R. Alonso-Mori, D. Nordlund, T.-C. Weng, D. Sokaras, F. Neese, U. Bergmann, V. K. Yachandra, S. DeBeer, V. L. Pecoraro and J. Yano, Inorg Chem **52** (22), 12915-12922 (2013).
46. E. P. Jahrman, W. M. Holden, A. S. Ditter, D. R. Mortensen, G. T. Seidler, T. T. Fister, S. A. Kozimor, L. F. J. Piper, J. Rana, N. C. Hyatt and M. C. Stennett, Review of Scientific Instruments **90** (2), 024106 (2019).
47. D. R. Mortensen, G. T. Seidler, J. J. Kas, N. Govind, C. P. Schwartz, S. Pemmaraju and D. G. Prendergast, Phys Rev B **96** (12), 125136 (2017).
48. W. Malzer, D. Grötzsch, R. Gnewkow, C. Schlesiger, F. Kowalewski, B. Van Kuiken, S. DeBeer and B. Kanngießer, Review of Scientific Instruments **89** (11), 113111 (2018).
49. L. Anklamm, C. Schlesiger, W. Malzer, D. Grötzsch, M. Neitzel and B. Kanngießer, Review of Scientific Instruments **85** (5), 053110 (2014).
50. R. Bès, T. Ahopelto, A. P. Honkanen, S. Huotari, G. Leinders, J. Pakarinen and K. Kvashnina, Journal of Nuclear Materials **507**, 50-53 (2018).
51. W. Błachucki, J. Czapla-Masztafiak, J. Sá and J. Szlachetko, Journal of Analytical Atomic Spectrometry **34** (7), 1409-1415 (2019).
52. W. M. Holden, O. R. Hoidn, A. S. Ditter, G. T. Seidler, J. Kas, J. L. Stein, B. M. Cossairt, S. A. Kozimor, J. Guo, Y. Ye, M. A. Marcus and S. Fakra, Review of Scientific Instruments **88** (7), 073904 (2017).
53. A.-P. Honkanen, S. Ollikkala, T. Ahopelto, A.-J. Kallio, M. Blomberg and S. Huotari, Review of Scientific Instruments **90** (3), 033107 (2019).
54. G. T. Seidler, D. R. Mortensen, A. J. Remesnik, J. I. Pacold, N. A. Ball, N. Barry, M. Styczinski and O. R. Hoidn, Review of Scientific Instruments **85** (11), 113906 (2014).
55. C. Sugiura, Y. Gohshi and I. Suzuki, Physical Review B **10** (2), 338-343 (1974).
56. Y. Gohshi, Y. Hukao and K. Hori, Spectrochimica Acta Part B: Atomic Spectroscopy **27** (3), 135-142 (1972).
57. S. Chikara, G. Yohichi and S. Isao, Jpn J Appl Phys **11** (6), 911 (1972).
58. M. Y. Yu, V. A. Trofimova, V. E. Dolgih, M. A. Korotin, E. Z. Kurmaev, J. A. Aguiar, J. M. Ferreira and A. C. Pavao, Journal of Physics: Condensed Matter **7** (1), 213 (1995).
59. Y. M. Yarmoshenko, V. A. Trofimova, E. Z. Kurmaev, P. R. Slater and C. Greaves, Physica C: Superconductivity **224** (3), 317-320 (1994).
60. Y. M. Yarmoshenko, V. A. Trofimova, L. V. Elokhina, E. Z. Kurmaev, S. Butorin, R. Cloots, M. Ausloos, J. A. Aguiar and N. I. Lobatchevskaya, Journal of Physics and Chemistry of Solids **54** (10), 1211-1214 (1993).
61. V. E. Dolgih, V. M. Cherkashenko, E. Z. Kurmaev, D. A. Goganov, E. K. Ovchinnikov and Y. M. Yarmoshienko, Nuclear Instruments and Methods in Physics Research **224** (1), 117-119 (1984).
62. M. Kavčič, J. C. Dousse, J. Szlachetko and W. Cao, Nuclear Instruments and Methods in Physics Research Section B: Beam Interactions with Materials and Atoms **260** (2), 642-646 (2007).
63. M. Szlachetko, M. Berset, J. C. Dousse, J. Hoszowska and J. Szlachetko, Rev Sci Instrum **84** (9), 093104 (2013).
64. Z. Németh, J. Szlachetko, É. G. Bajnóczi and G. Vankó, Review of Scientific Instruments **87** (10), 103105 (2016).
65. Y. Kayser, W. Błachucki, J. C. Dousse, J. Hoszowska, M. Neff and V. Romano, Rev Sci Instrum **85** (4), 043101 (2014).
66. J. Hoszowska, J. C. Dousse, J. Kern and C. Rhême, Nuclear Instruments and Methods in Physics Research Section A: Accelerators, Spectrometers, Detectors and Associated Equipment **376** (1), 129-138 (1996).
67. R. A. Valenza, E. P. Jahrman, J. J. Kas and G. T. Seidler, Phys Rev A **96** (3), 032504 (2017).

68. G. T. Seidler, D. R. Mortensen, A. S. Ditter, N. A. Ball and A. J. Remesnik, Journal of Physics: Conference Series **712** (1), 012015 (2016).
69. D. R. Mortensen, G. T. Seidler, A. S. Ditter and P. Glatzel, Journal of Physics: Conference Series **712** (1), 012036 (2016).
70. D. R. Mortensen and G. T. Seidler, J Electron Spec **215**, 8-15 (2017).
71. E. P. Jahrman, G. T. Seidler and J. R. Sieber, Anal Chem **90** (11), 6587-6593 (2018).
72. J. G. Moya-Cancino, A.-P. Honkanen, A. M. J. van der Eerden, H. Schaink, L. Folkertsma, M. Ghiasi, A. Longo, F. M. F. de Groot, F. Meirer, S. Huotari and B. M. Weckhuysen, ChemCatChem **11** (3), 1039 (2019).
73. M. E. Mundy, D. Ung, N. L. Lai, E. P. Jahrman, G. T. Seidler and B. M. Cossairt, Chem Mater **30** (15), 5373 (2018).
74. S. I. Kalläne, A. W. Hahn, T. Weyhermüller, E. Bill, F. Neese, S. DeBeer and M. van Gastel, Inorg Chem **58** (8), 5111-5125 (2019).
75. M. A. Beckwith, M. Roemelt, M.-N. Collomb, C. DuBoc, T.-C. Weng, U. Bergmann, P. Glatzel, F. Neese and S. DeBeer, Inorganic Chemistry **50** (17), 8397-8409 (2011).
76. G. Smolentsev, A. V. Soldatov, J. Messinger, K. Merz, T. Weyhermüller, U. Bergmann, Y. Pushkar, J. Yano, V. K. Yachandra and P. Glatzel, Journal of the American Chemical Society **131** (36), 13161-13167 (2009).
77. S. C. E. Stieber, C. Milsmann, J. M. Hoyt, Z. R. Turner, K. D. Finkelstein, K. Wieghardt, S. DeBeer and P. J. Chirik, Inorganic Chemistry **51** (6), 3770-3785 (2012).
78. O. Bunău and Y. Joly, Physical Review B **85** (15), 155121 (2012).
79. P. Elliott, F. Furche and K. Burke, Reviews in Computational Chemistry, 91-165 (2008).
80. K. A. Lopata, B. E. Van Kuiken, M. Khalil and N. Govind, Journal of Chemical Theory and Computation, 8(9):3284-3292 **8** (9) (2012).
81. Y. Zhang, S. Mukamel, M. Khalil and N. Govind, Journal of Chemical Theory and Computation **11** (12), 5804-5809 (2015).
82. M. Valiev, E. J. Bylaska, N. Govind, K. Kowalski, T. P. Straatsma, H. J. J. Van Dam, D. Wang, J. Nieplocha, E. Apra, T. L. Windus and W. A. de Jong, Computer Physics Communications **181** (9), 1477-1489 (2010).
83. W. M. Holden, E. P. Jahrman, N. Govind and G. T. Seidler, (Submitted).
84. L. Burkhardt, M. Holzwarth, B. Plietker and M. Bauer, Inorg Chem **56** (21), 13300-13310 (2017).
85. L. Burkhardt, C. Mueller, O. A. Groß, Y. Sun, H. Sitzmann and M. Bauer, Inorg Chem **58** (10), 6609-6618 (2019).
86. S. DeBeer George, T. Petrenko and F. Neese, Inorganica Chimica Acta **361** (4), 965-972 (2008).
87. N. Govind, K. Lopata, R. Rousseau, A. Andersen and K. Kowalski, The Journal of Physical Chemistry Letters **2** (21), 2696-2701 (2011).
88. P. J. Lestrange, P. D. Nguyen and X. Li, Journal of Chemical Theory and Computation **11** (7), 2994-2999 (2015).
89. M. J. Powell, I. J. Godfrey, R. Quesada-Cabrera, D. Malarde, D. Teixeira, H. Emerich, R. G. Palgrave, C. J. Carmalt, I. P. Parkin and G. Sankar, The Journal of Physical Chemistry C **121** (37), 20345-20352 (2017).
90. B. Ravel and M. Newville, Journal of Synchrotron Radiation **12** (4), 537-541 (2005).
91. C. M. Teodorescu, G. Socol, C. Negrila, D. Luca and D. Macovei, Journal of Experimental Nanoscience **5** (6), 509-526 (2010).
92. M. Bianchini, J. M. Ateba-Mba, P. Dagault, E. Bogdan, D. Carlier, E. Suard, C. Masquelier and L. Croguennec, Journal of Materials Chemistry A **2** (26), 10182-10192 (2014).
93. D. Kriegner, E. Wintersberger and J. Stangl, Journal of Applied Crystallography **46** (4), 1162-1170 (2013).

94. H. Enkisch, C. Sternemann, M. Paulus, M. Volmer and W. Schulke, Phys Rev A **70** (2), 022508 (2004).
95. M. Casarin, C. Maccato and A. Vittadini, The Journal of Physical Chemistry B **102** (52), 10745-10752 (1998).
96. M. L. Sushko, A. Y. Gal and A. L. Shluger, The Journal of Physical Chemistry B **110** (10), 4853-4862 (2006).
97. L.-W. Wang and J. Li, Physical Review B **69** (15), 153302 (2004).
98. J. D. Wadey and N. A. Besley, Journal of Chemical Theory and Computation **10** (10), 4557-4564 (2014).
99. C. Adamo and V. Barone, The Journal of Chemical Physics **110** (13), 6158-6170 (1999).
100. T. H. Dunning and P. J. Hay, in *Methods of Electronic Structure Theory*, edited by H. F. Schaefer (Springer US, Boston, MA, 1977), pp. 1-27.
101. J. D. Dill and J. A. Pople, The Journal of Chemical Physics **62** (7), 2921-2923 (1975).
102. V. A. Rassolov, J. A. Pople, M. A. Ratner and T. L. Windus, The Journal of Chemical Physics **109** (4), 1223-1229 (1998).
103. A. Bergner, M. Dolg, W. Küchle, H. Stoll and H. Preuß, Molecular Physics **80** (6), 1431-1441 (1993).
104. P. J. Hay and W. R. Wadt, The Journal of Chemical Physics **82** (1), 299-310 (1985).
105. T. Noro, M. Sekiya and T. Koga, Theoretical Chemistry Accounts **131** (2), 1124 (2012).
106. H.-G. Bachmann, F. R. Ahmed and W. H. Barnes, Zeitschrift fuer Kristallographie **115** (1), 110-131 (1961).
107. Y. Ding, C.-C. Chen, Q. Zeng, H.-S. Kim, M. J. Han, M. Balasubramanian, R. Gordon, F. Li, L. Bai, D. Popov, S. M. Heald, T. Gog, H.-K. Mao and M. van Veenendaal, Phys Rev Lett **112** (5) (2014).
108. M. Francis V. Hidalgo, Y.-C. Lin, A. Grenier, D. Xiao, J. Rana, R. Tran, H. Xin, M. Zuba, J. Donohue, F. O. Omenya, I.-H. Chu, Z. Wang, X. Li, N. A. Chernova, K. W. Chapman, G. Zhou, L. Piper, S. P. Ong and M. S. Whittingham, Journal of Materials Chemistry A **7** (14), 8423-8432 (2019).
109. G. V. Subba Rao and C. N. R. Rao, *Transition metal oxides: crystal chemistry, phase transition, and related aspects*. (Washington: U.S. Dept. of Commerce, National Bureau of Standards, 1974).
110. H. Ågren, V. Carravetta, O. Vahtras and L. G. M. Pettersson, Chem Phys Lett **222** (1), 75-81 (1994).
111. H. Ågren, V. Carravetta, O. Vahtras and L. G. M. Pettersson, Theoretical Chemistry Accounts **97** (1), 14-40 (1997).
112. W. J. Hunt and W. A. Goddard, Chem Phys Lett **3** (6), 414-418 (1969).
113. H. F. King, R. E. Stanton, H. Kim, R. E. Wyatt and R. G. Parr, The Journal of Chemical Physics **47** (6), 1936-1941 (1967).
114. P. G. Lykos and H. N. Schmeising, The Journal of Chemical Physics **35** (1), 288-293 (1961).
115. S. Hirata and M. Head-Gordon, Chem Phys Lett **314** (3), 291-299 (1999).
116. T. Mukoyama, Spectrochimica Acta Part B: Atomic Spectroscopy **59** (8), 1107-1115 (2004).
117. J. J. Rehr and R. C. Albers, Reviews of Modern Physics **72** (3), 621-654 (2000).
118. J. J. Rehr, J. J. Kas, M. P. Prange, A. P. Sorini, Y. Takimoto and F. Vila, Comptes Rendus Physique **10** (6), 548-559 (2009).
119. J. J. Rehr, J. J. Kas, F. D. Vila, M. P. Prange and K. Jorissen, Phys Chem Chem Phys **12** (21), 5503-5513 (2010).
120. J. A. Rees, A. Wandzilak, D. Maganas, N. I. C. Wurster, S. Hugenbruch, J. K. Kowalska, C. J. Pollock, F. A. Lima, K. D. Finkelstein and S. DeBeer, JBIC Journal of Biological Inorganic Chemistry **21** (5), 793-805 (2016).
121. Y. Guo, S. J. Clark and J. Robertson, The Journal of Chemical Physics **140** (5), 054702 (2014).
122. A. Haras, M. Witko, D. R. Salahub, K. Hermann and R. Tokarz, Surf Sci **491** (1), 77-87 (2001).

123. F. D. Hardcastle and I. E. Wachs, The Journal of Physical Chemistry **95** (13), 5031-5041 (1991).
124. R. A. Mori, E. Paris, G. Giuli, S. G. Eeckhout, M. Kavčič, M. Žitnik, K. Bučar, L. G. M. Pettersson and P. Glatzel, Inorganic Chemistry **49** (14), 6468-6473 (2010).
125. B. Lassalle-Kaiser, T. T. Boron, V. Krewald, J. Kern, M. A. Beckwith, M. U. Delgado-Jaime, H. Schroeder, R. Alonso-Mori, D. Nordlund, T.-C. Weng, D. Sokaras, F. Neese, U. Bergmann, V. K. Yachandra, S. DeBeer, V. L. Pecoraro and J. Yano, Inorganic Chemistry **52** (22), 12915-12922 (2013).
126. U. Bergmann, P. Glatzel, F. deGroot and S. P. Cramer, Journal of the American Chemical Society **121** (20), 4926-4927 (1999).
127. U. Bergmann, P. Glatzel, J. H. Robblee, J. Messinger, C. Fernandez, R. Cinco, H. Visser, K. McFarlane, E. Bellacchio, S. Pizarro, K. Sauer, V. K. Yachandra, M. P. Klein, B. L. Cox, K. H. Nealson and S. P. Cramer, Journal of synchrotron radiation **8** (Pt 2), 199-203 (2001).
128. J. Chakhalian, J. M. Rondinelli, J. Liu, B. A. Gray, M. Kareev, E. J. Moon, N. Prasai, J. L. Cohn, M. Varela, I. C. Tung, M. J. Bedzyk, S. G. Altendorf, F. Strigari, B. Dabrowski, L. H. Tjeng, P. J. Ryan and J. W. Freeland, Phys Rev Lett **107** (11), 116805 (2011).
129. C. A. Marianetti, G. Kotliar and G. Ceder, Phys Rev Lett **92** (19), 196405 (2004).
130. J. Suntivich, H. A. Gasteiger, N. Yabuuchi, H. Nakanishi, J. B. Goodenough and Y. Shao-Horn, Nature Chemistry **3** (7), 546-550 (2011).
131. J. Suntivich, W. T. Hong, Y.-L. Lee, J. M. Rondinelli, W. Yang, J. B. Goodenough, B. Dabrowski, J. W. Freeland and Y. Shao-Horn, The Journal of Physical Chemistry C **118** (4), 1856-1863 (2014).
132. C. J. Ballhausen, *Introduction to ligand field theory*. (New York : McGraw-Hill Book Company, Inc., New York, 1962).
133. T. Sudayama, K. Uehara, T. Mukai, D. Asakura, X.-M. Shi, A. Tsuchimoto, B. Mortemard de Boisse, T. Shimada, E. Watanabe, Y. Harada, M. Nakayama, M. Okubo and A. Yamada, Energy & Environmental Science **13** (5), 1492-1500 (2020).
134. X. Wang, X. Fan, X. Yu, S. Bak, Z. Shadike, I. Waluyo, A. Hunt, S. D. Senanayake, H. Li, L. Chen, C. Wang, R. Xiao, E. Hu and X.-Q. Yang, Advanced Functional Materials **n/a** (n/a), 2001633 (2020).
135. C. F. Petersburg, Z. Li, N. A. Chernova, M. S. Whittingham and F. M. Alamgir, Journal of Materials Chemistry **22** (37), 19993-20000 (2012).
136. U. Bergmann, J. Bendix, P. Glatzel, H. B. Gray and S. P. Cramer, The Journal of Chemical Physics **116** (5), 2011-2015 (2002).
137. J. Herrero-Martín, A. Mirone, J. Fernández-Rodríguez, P. Glatzel, J. García, J. Blasco and J. Geck, Physical Review B **82** (7), 075112 (2010).
138. D. Maganas, S. DeBeer and F. Neese, Inorganic Chemistry **56** (19), 11819-11836 (2017).
139. C. J. Pollock, K. M. Lancaster, K. D. Finkelstein and S. DeBeer, Inorganic Chemistry **53** (19), 10378-10385 (2014).
140. D.-H. Seo, J. Lee, A. Urban, R. Malik, S. Kang and G. Ceder, Nature Chemistry **8** (7), 692-697 (2016).
141. M. Cavalleri, K. Hermann, A. Knop-Gericke, M. Hävecker, R. Herbert, C. Hess, A. Oestereich, J. Döbler and R. Schlögl, Journal of Catalysis **262** (2), 215-223 (2009).
142. C. Kolczewski and K. Hermann, Surface Science **552** (1), 98-110 (2004).
143. D. Maganas, M. Roemelt, M. Hävecker, A. Trunschke, A. Knop-Gericke, R. Schlögl and F. Neese, Physical Chemistry Chemical Physics **15** (19), 7260-7276 (2013).
144. M. Tian, C. Liu, J. Zheng, X. Jia, E. P. Jahrman, G. T. Seidler, D. Long, M. Atif, M. Alsalhi and G. Cao, Energy Storage Materials **29**, 9-16 (2020).
145. J. Zheng, C. Liu, M. Tian, X. Jia, E. P. Jahrman, G. T. Seidler, S. Zhang, Y. Liu, Y. Zhang, C. Meng and G. Cao, Nano Energy **70**, 104519 (2020).
146. E. P. Jahrman, L. A. Pellerin, A. S. Ditter, L. R. Bradshaw, T. T. Fister, B. J. Polzin, S. E. Trask, A. R. Dunlop and G. T. Seidler, Journal of The Electrochemical Society **166** (12), A2549-A2555 (2019).

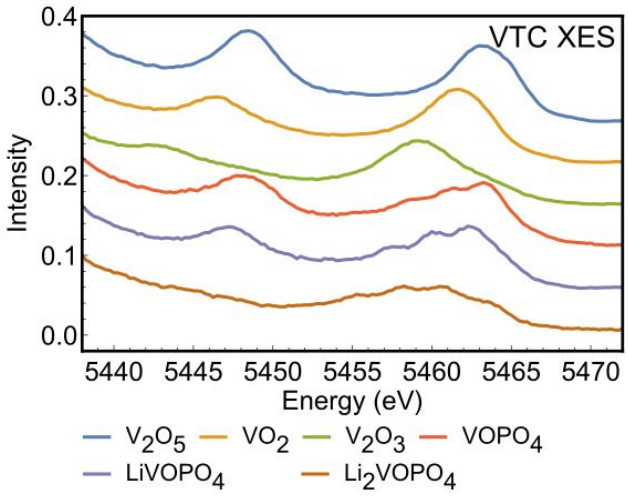

Fig. 1: Experimental V VTC-XES spectra of the set of V oxides and vanadyl phosphates. Spectra are shown after deadtime correction, constant background subtraction and integral normalization over the entire scan range. Spectra are vertically offset for comparison.

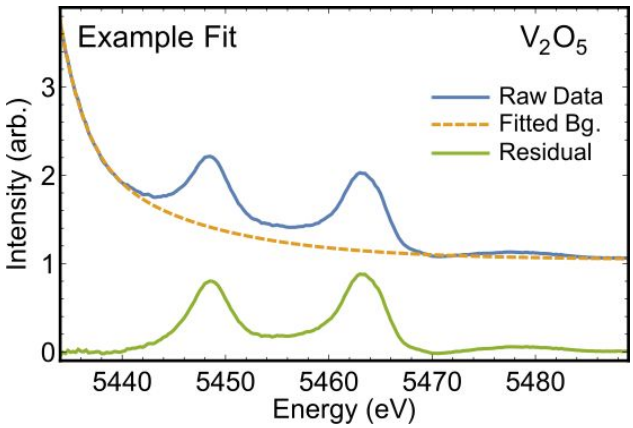

Fig. 2: Representative experimental V VTC-XES results are shown for V_2O_5 (blue) along with the background fit to the low- and high-energy ranges of the VTC (orange, dashed). These two spectra are shown offset from the residual (green). The residual represents the VTC-XES without the tail from the V $K\beta_{1,3}$.

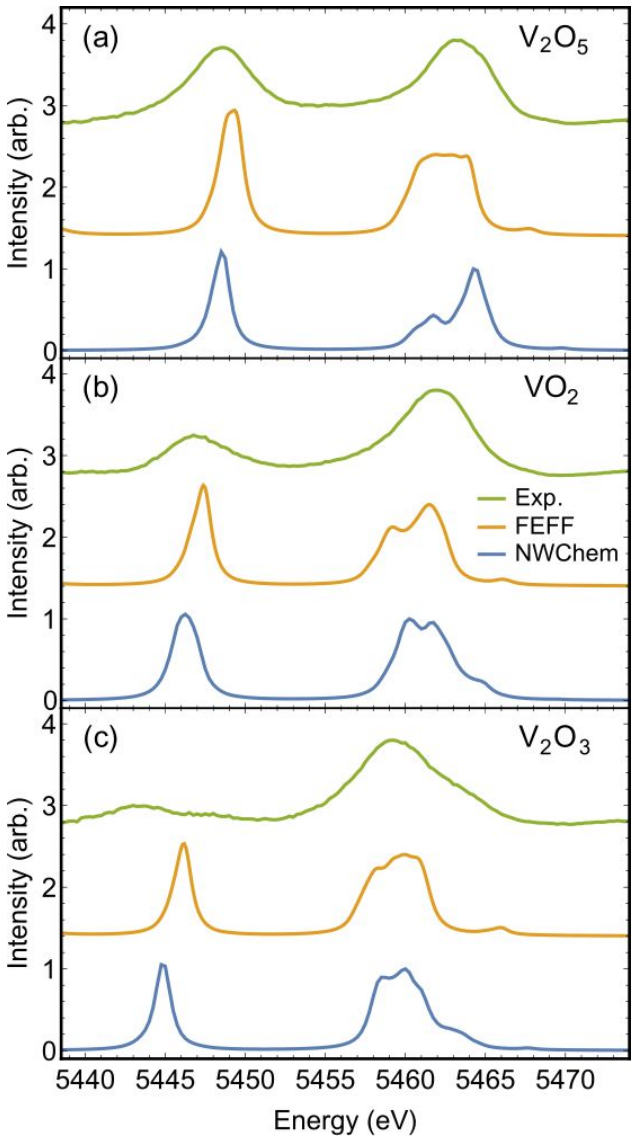

Fig. 3: V VTC-XES results for a suite of V oxides. The top spectrum in each frame is the experimental spectrum after subtraction of the tail from the V $K\beta_{1,3}$. The middle spectrum in each frame is the spectrum calculated by `FEFF9` using a Green's function approach. The bottom spectrum in each frame is the spectrum calculated by `NWChem` using a TDDFT approach.

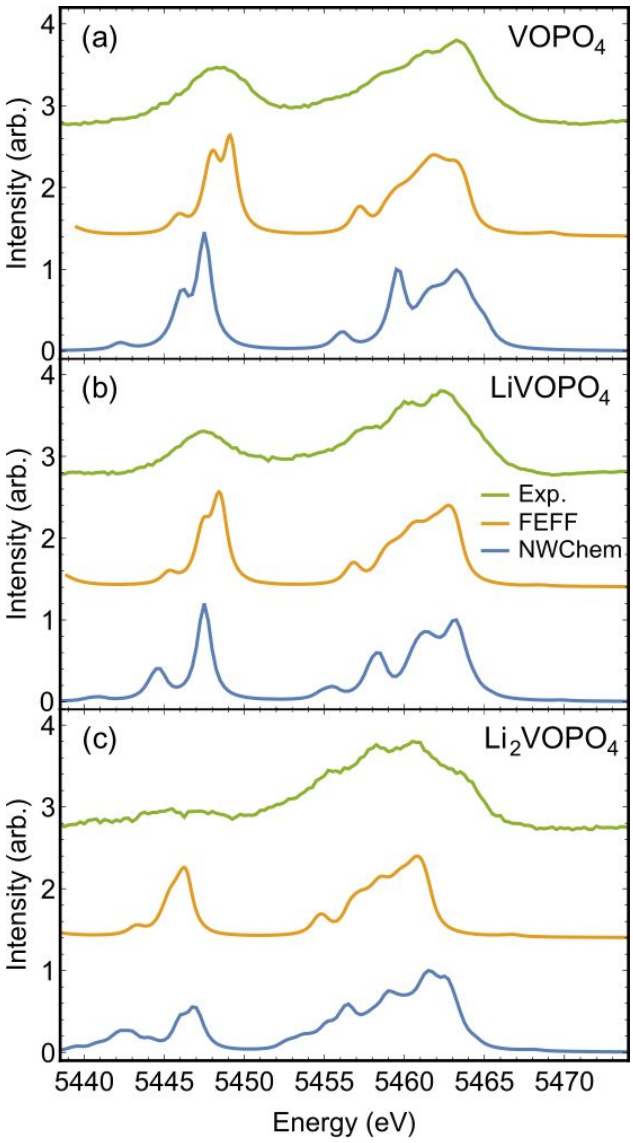

Fig. 4: V VTC-XES results for a suite of vanadyl phosphates. The top spectrum in each frame is the experimental spectrum after subtraction of the tail from the V $K\beta_{1,3}$. The middle spectrum in each frame is the spectrum calculated by `FEFF9` using a Green's function approach. The bottom spectrum in each frame is the spectrum calculated by `NWChem` using a TDDFT approach.

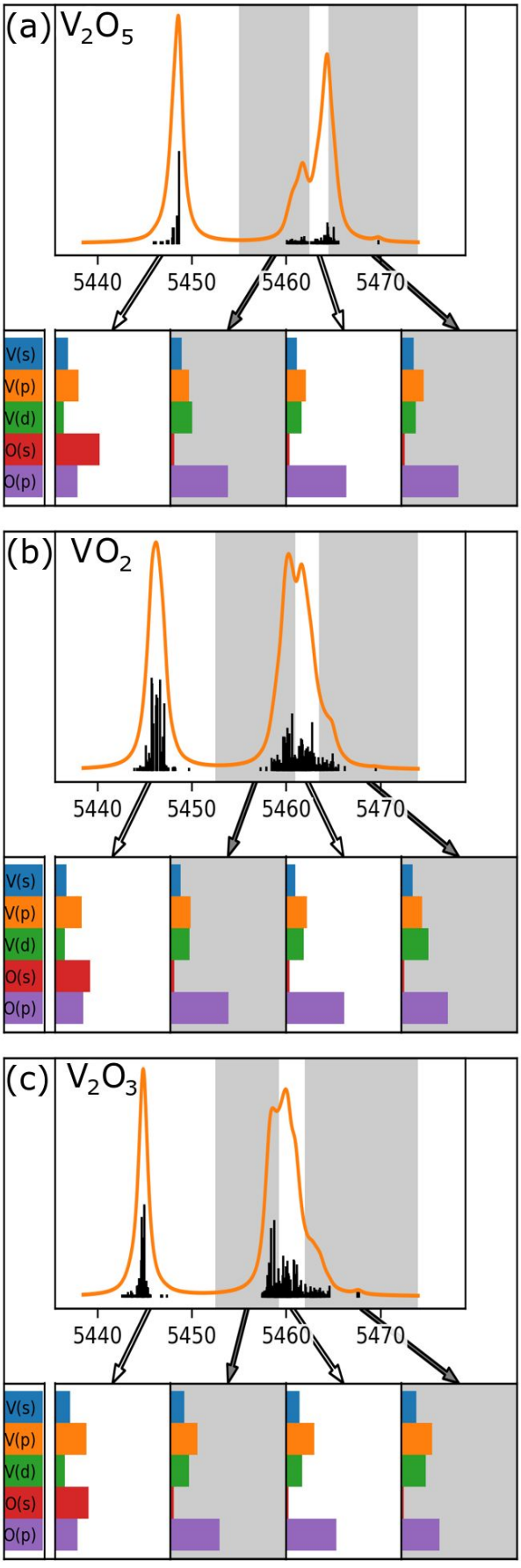
(a) V_2O_5
5440
5450
5460
5470
V(s)
V(p)
V(d)
O(s)
O(p)
(b) VO_2
5440
5450
5460
5470
V(s)
V(p)
V(d)
O(s)
O(p)
(c) V_2O_3
5440
5450
5460
5470
V(s)
V(p)
V(d)
O(s)
O(p)

Fig. 5: Calculated VTC-XES results using TDDFT for the oxide-based samples. The bar plots below each spectrum represent each orbital-type's contribution to the roots in the associated energy region. Quantities on the x- and y-axes are the same as in Fig. 3.

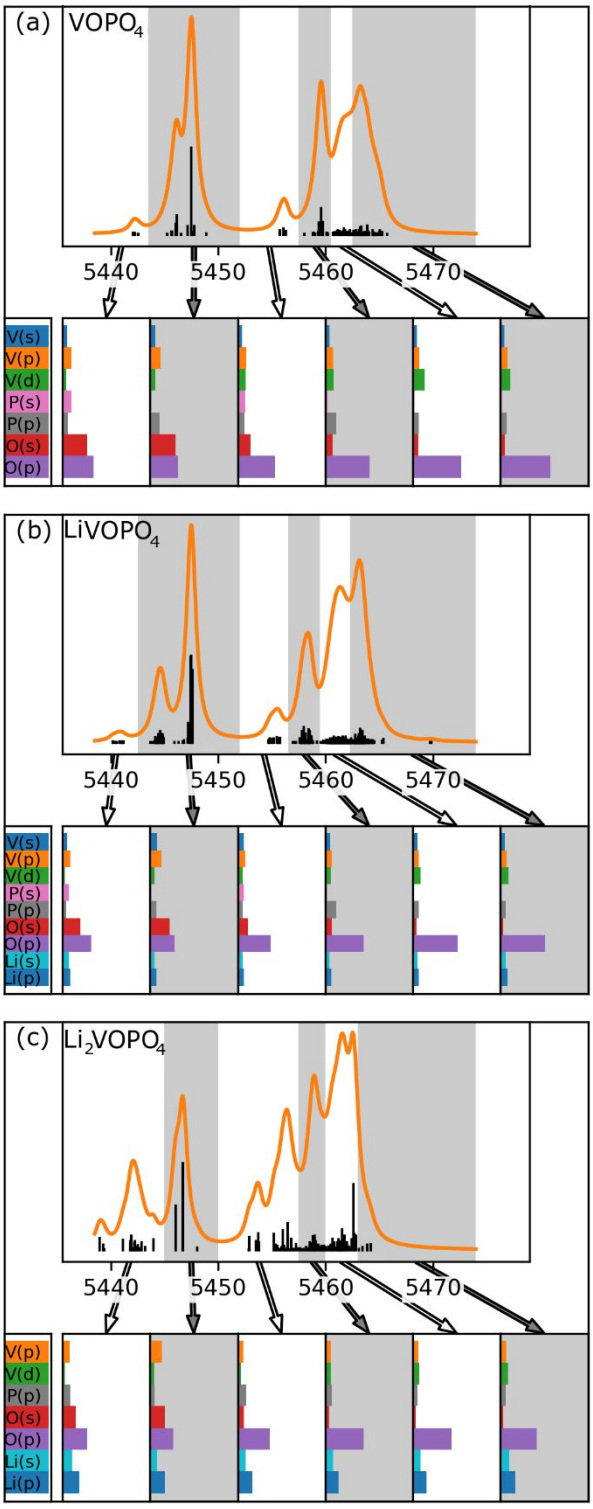
(a) VOPO4
5440
5450
5460
5470
V(s)
V(p)
V(d)
P(s)
P(p)
O(s)
O(p)
(b) LiVOPO4
5440
5450
5460
5470
V(s)
V(p)
V(d)
P(s)
P(p)
O(s)
O(p)
Li(s)
Li(p)
(c) Li2VOPO4
5440
5450
5460
5470
V(p)
V(d)
P(p)
O(s)
O(p)
Li(s)
Li(p)

Fig. 6: Calculated VTC-XES results using TDDFT for the phosphate-based samples. The bar plots below each spectrum represent each orbital-type's contribution to the roots in the associated energy region. Quantities on the x- and y-axes are the same as in Fig. 4.

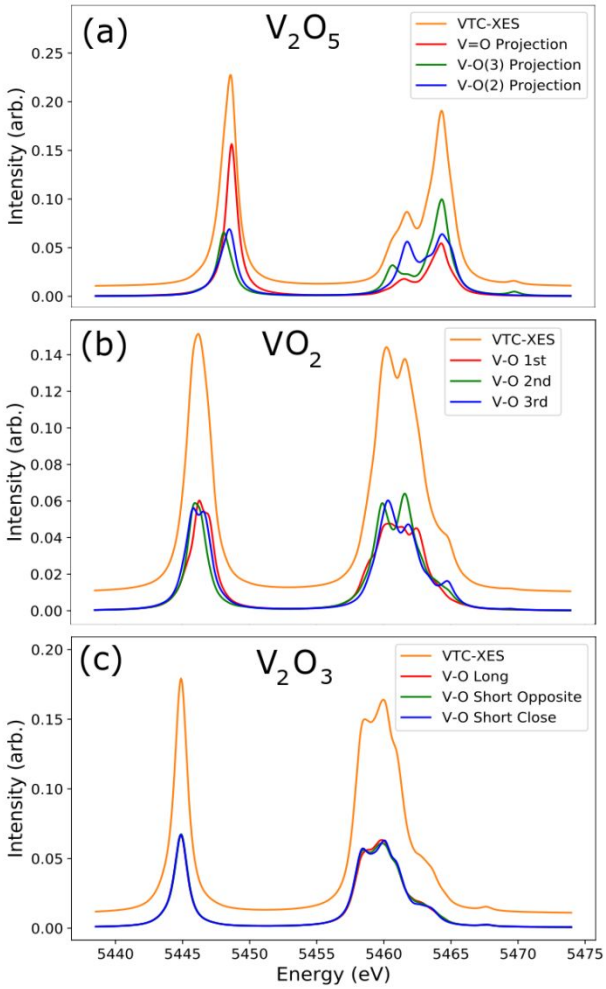

Fig. 7: Theoretical V VTC-XES spectra (orange, offset for clarity) and the transition dipole moment contributions of non-orthogonal polarizations in the direction of three different ligands coordinating the central V atom. These directions can be found in Fig. S1. The components of a given spectrum were scaled consistently relative to one another, but given an arbitrary overall scaling. (a) Polarizations were chosen along the doubly-bonded oxygen (V=O Projection), the singly-bonded oxygen with a coordination number of three (V-O(3) Projection), and the singly-bonded oxygen with a coordination number of two (V-O(2) Projection). (b) Decompositions are provided in the direction of the three singly-bonded oxygens on the corners of the irregular octahedron. The decompositions are provided in order of increasing bond length: 1.90, 2.05, and

2.14 Å, respectively. (c) Decompositions are provided in the direction of the three singly-bonded oxygens on the corners of the irregular tetrahedron. The decompositions are provided for a singly-bonded oxygen at 2.05 Å (V-O Long), and two singly-bonded oxygens at 1.97 Å that were either in the plane of atoms closest to the oxygen associated with V-O Long (V-O Short Close) or opposite it (V-O Short Far).

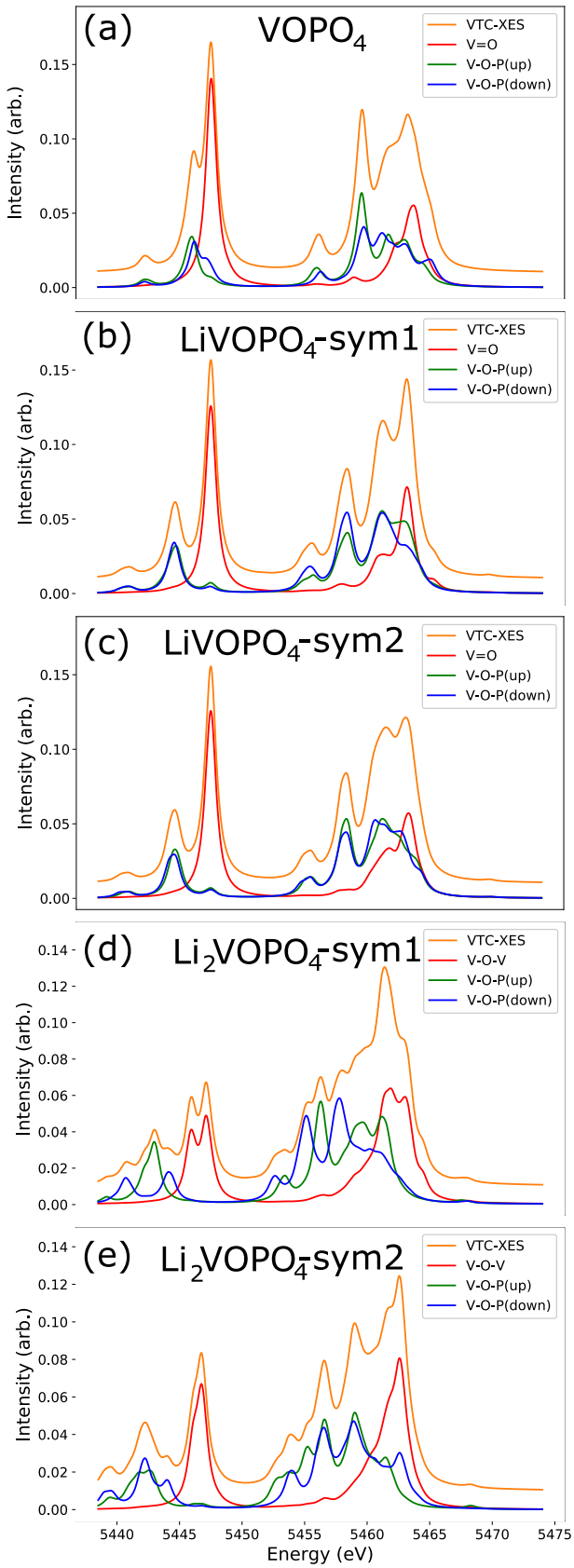
(a) VOPO4
VTC-XES
V=O
V-O-P(up)
V-O-P(down)
(b) LiVOPO4-sym1
VTC-XES
V=O
V-O-P(up)
V-O-P(down)
(c) LiVOPO4-sym2
VTC-XES
V=O
V-O-P(up)
V-O-P(down)
(d) Li2VOPO4-sym1
VTC-XES
V-O-V
V-O-P(up)
V-O-P(down)
(e) Li2VOPO4-sym2
VTC-XES
V-O-V
V-O-P(up)
V-O-P(down)
Intensity (arb.)
Energy (eV)
5440
5445
5450
5455
5460
5465
5470
5475

Fig. 8: Theoretical V VTC-XES spectra (orange, offset for clarity) and the transition dipole moment contributions of non-orthogonal polarizations in the direction of three different ligands coordinating the central V atom. These directions can be found in Fig. S2. The components of a given spectrum were scaled consistently relative to one another, but given an arbitrary overall scaling. (a) Polarizations of $VOPO_4$ were chosen along the doubly-bonded oxygen (V=O) and two adjacent singly-bonded oxygens belonging to phosphate groups. The first singly-bonded oxygen belonged to a phosphate group with its vertex directed upward with respect to the direction of the doubly-bonded oxygen (V-O-P(up)) and the second singly-bonded oxygen belonged to a phosphate group with its vertex directed downward (V-O-P(down)). (b) Projections are shown for the first unique symmetry site of V in $LiVOPO_4$. The same conventions are used to designate the projections as in part a. (c) Projections are shown for the second unique symmetry site of V in $LiVOPO_4$. The same conventions are used to designate the projections as in part a. (d-e) Parts d and e are the Li_2VOPO_4 analogs of b and c. In this case, there is not a clear V=O group, rather two oxygen atoms are located above and below the central V atom and bridge it to another V atom. One of these directions was chosen and is designated as (V-O-V). V-O-P(up) and V-O-P(down) are specified relative the direction of V-O-V.

Sentence Summary:

Coupling lab-based XES measurements with computations amenable to solid-state systems revealed the valence band behavior of several vanadium-based electronic materials.

TOC graphic: